Elementary processes in BeH^+ molecular plasma

S. NIYONZIMA[1,2] , F. LIQUE[1], K. CHAKRABARTI[3,1], A. LARSON[4], and I. F. SCHNEIDER[1]

[1]LOMC, UMR 6294, CNRS-Université du Havre 76058 Le Havre, France
[2]Département de Physique, Faculté des Sciences, Université du Burundi, 2700 Bujumbura, Burundi
[3]Dept. Of Mathematics, Scottish Church College, 1&3 Urquhart Sq., Kolkata 700 006, India.
[4]Department of Physics, Stockholm University, AlbaNova University Center, S-106 91 Stockholm,Sweden

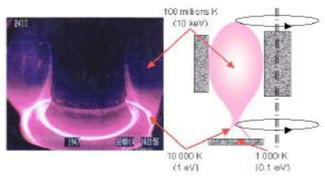

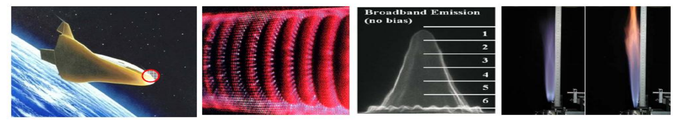

1. Introduction

According to the design of the International Tokamak Experiment Reactor (ITER), Beryllium have been chosen as a plasma facing material [1-7]. Hydrogen, Deuterium and Tritium will form with Beryllium different molecular species in plasma state. In order to model the kinetics of this environment and the plasma-wall interactions in ITER, it is crucial to describe the elementary processes involving these molecules. BeH^+ can be destroyed by Dissociative Recombination (DR) [2]:

$$BeH^+ + e^- \rightarrow BeH^{**}, BeH^* \rightarrow Be + H \qquad (1)$$

assisted by Vibrational Excitation (VE):

$$BeH^+ + e^- \rightarrow BeH^{**}, BeH^* \rightarrow e^- + BeH^{+*} \qquad (2)$$

Two mechanisms govern these processes: the *direct* one, consisting in the capture into a dissociative state BeH**, and the *indirect* one, relying on temporary captures into bound Rydberg states BeH*, predissociated by BeH**.

No measurement of the DR rate of BeH^+ is available, due to its high toxicity. Nevertheless, first theoretical estimations have been performed recently [2] using the wave-packet method (WPM). In order to better account for the role of the indirect process, we have employed the molecular data produced within this previous study in a new series of computations relying on a method [8, 9] based on the Multichannel Quantum Defect Theory(MQDT). We present the determination of DR cross sections and rate coefficients at low, intermediate and high energy/temperature.

2. Molecular Data

We have used the molecular data of Roos et al. [2]. Three symmetries $^2\Pi$, $^2\Sigma^+$, and $^2\Delta$ of BeH have been taken into account. Potential energies curves (PEC) of each symmetries have been determined using the Multireference Configuration Interaction (MRCI) followed by a diabatization procedure. The quantum defect have been extracted applying Rydberg formula for the bound states.

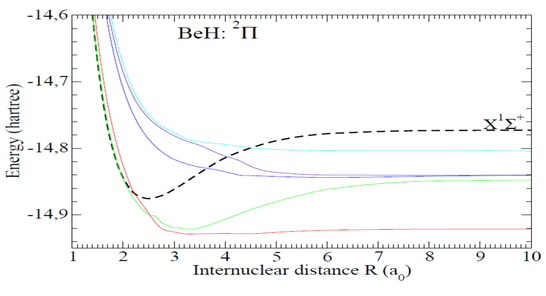

Fig.1: Potential energy curves of BeH in $^2\Pi$ symmetry[2]

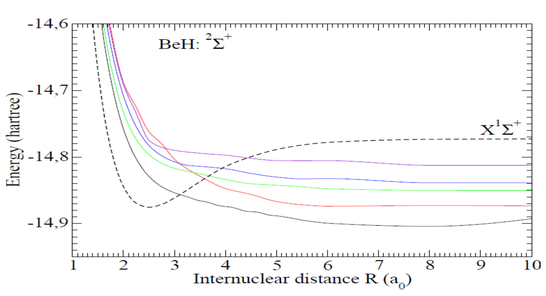

Fig. 2: Potential energy curves of BeH in $^2\Sigma^+$ symmetry[2]

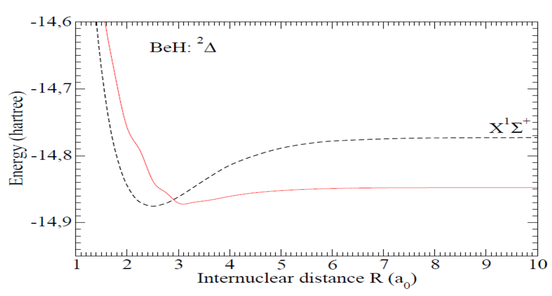

Fig.3: Potential energy curve of BeH in $^2\Delta$ symmetry [2]

3. Multichannel Quantum Defect Theory(MQDT) [8-13]

1° Construction of the interaction matrix:

$$\mathcal{V}_{d_j,v^+}(E) = \langle \chi_{d_j} \mid V(R) \mid \chi_{v^+} \rangle \qquad (3)$$

2°Construction of the reaction matrix:

$$\mathcal{K} = \mathcal{V} + \mathcal{V}\frac{1}{E - H_0}\mathcal{K} \qquad (4)$$

3° Diagonalization of the reaction matrix:

$$\boldsymbol{\mathcal{K}\mathcal{U}} = -\frac{1}{\pi}\tan(\boldsymbol{\eta})\boldsymbol{\mathcal{U}} \qquad (5)$$

4° Frame-transformation coefficients:

$$\mathcal{C}_{lv^+,\Lambda\alpha} = \sum_v U^{\Lambda}_{lv,\alpha} \langle \chi_{v^+}(R) | \cos(\pi\mu_l^{\Lambda}(R) + \eta_\alpha^{\Lambda}) | \chi_v(R) \rangle \qquad (6)$$

$$\mathcal{C}_{d,\Lambda\alpha} = U^{\Lambda}_{d\alpha}\cos\eta^{\Lambda}_{\alpha} \qquad (7)$$

5° Construction of the generalized scattering matrix:

$$\boldsymbol{X} = \frac{\boldsymbol{\mathcal{C}} + i\boldsymbol{\mathcal{S}}}{\boldsymbol{\mathcal{C}} - i\boldsymbol{\mathcal{S}}}, \qquad \boldsymbol{X} = \begin{pmatrix} \boldsymbol{X}_{oo} & \boldsymbol{X}_{oc} \\ \boldsymbol{X}_{co} & \boldsymbol{X}_{cc} \end{pmatrix} \qquad (8)$$

The ***S*** elements in (8) are obtained by replacing cos by sin in (6) and (7).

6° Elimination of closed channels:

$$\boldsymbol{S} = \boldsymbol{X}_{oo} - \boldsymbol{X}_{oc}\frac{1}{\boldsymbol{X}_{cc} - \exp(-\mathrm{i}2\pi\boldsymbol{\nu})}\boldsymbol{X}_{co} \qquad (9)$$

7° Evaluation of DR&VE partial and global cross section:

DR: $$\sigma^{sym,\Lambda}_{diss\leftarrow v_i^+} = \frac{\pi}{4\varepsilon}\rho^{sym,\Lambda}\sum_{l,j}|S_{d_j,lv_i^+}|^2 \qquad (10)$$

$$\sigma^{sym}_{diss\leftarrow v_i^+} = \sum_{\Lambda}\sigma^{sym,\Lambda}_{diss\leftarrow v_i^+} \qquad (11)$$

VE: $$\sigma^{sym,\Lambda}_{v_f^+\leftarrow v_i^+} = \frac{\pi}{4\varepsilon}\rho^{sym,\Lambda}\sum_{l,l'} \mid S_{l'v_f^+,lv_i^+} \mid^2 \qquad (12)$$

$$\sigma^{sym}_{v_f^+\leftarrow v_i^+} = \sum_{\Lambda}\sigma^{sym,\Lambda}_{v_f^+\leftarrow v_i^+} \qquad (13)$$

4. DR and VE cross sections

Assuming BeH^+ in its ground state ($X^1\Sigma^+, v_i = 0$), we have performed a series of MQDT calculations of DR and VE cross sections exploring for the energy range of the incident electron, the interval 0-2.7eV. We represent these cross sections on the following figures.

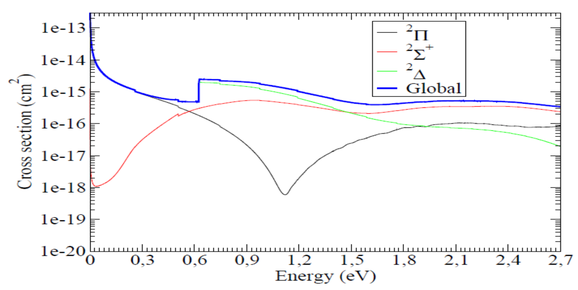

Fig.4. **DR:** Contribution of each symmetry

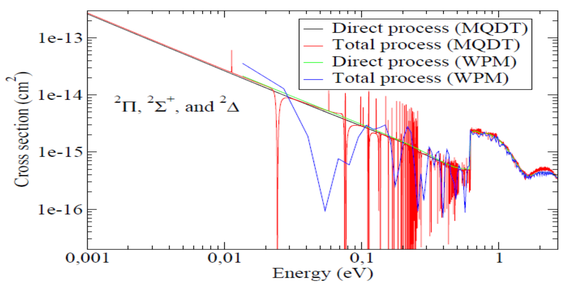

Fig.5. Comparison MQDT/WPM

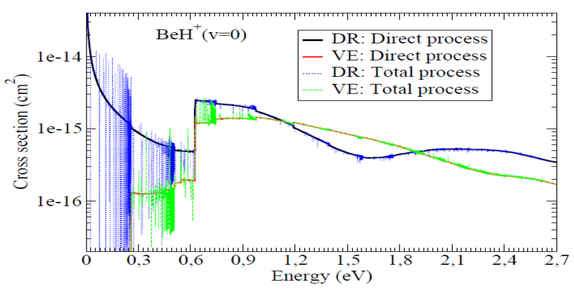

Fig.6. Competition DR/VE

6. Discussion

Figure 4 gives the direct cross section – global and for each symmetry. The $^2\Pi$ symmetry dominates the process because the potential energy curves of the corresponding first and second dissociative states cross the ion potential curve near the equilibrium internuclear distance (Fig.1). Figure 5 highlights Rydberg resonances which are found by the two approaches (wave-packet and MQDT). Through the same figure, it is clear that the wave-packet technique is not accurate at low collision energy because of difficulties in damping outgoing waves. Figures 6 and 7 show the strong competition between DR and VE processes at intermediate and high energy/temperature. Figures 7 and 8 display the Maxwellian rate coefficients (direct and total, - i.e. direct and indirect – within the two approaches). Slight differences between the DR rates occur at very low energy, where the MQDT is more appropriated.

7. Conclusions

Wave Packet and MQDT approaches agree well at high energy. At low energy, MQDT is more appropriate, the total (direct and indirect) rate being in the same order of magnitude as the direct one. Our MQDT computations of DR cross sections and rates, valid down to zero energy of incident electron complete the previous wave-packet calculations [2] and support them at intermediate energy. These results would help in modelling the plasma-wall interaction in the fusion devices involving BeH^+.

5. Rate coefficients

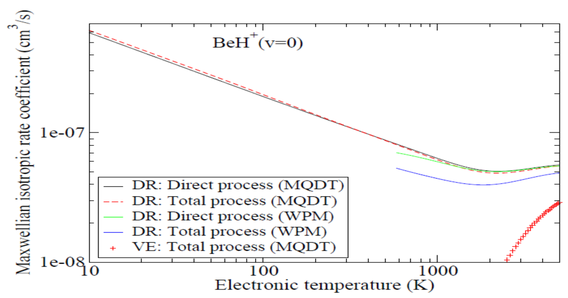

Fig.7. Comparison of rate coefficients

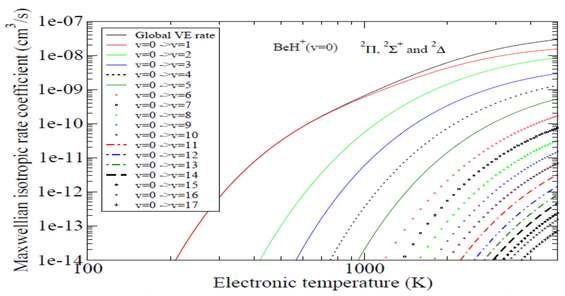

Fig.8. Global and individual VE rate coefficient

References

[1] Clark R.E.H. & Reiter D.H**. Nuclear Fusion Research** Understanding Plasma-surface Interactions**,** Springer Series in **CHEMICAL PHYSICS 78** , Berlin, 2005.
[2] Roos J.B., Larsson. M, Orel A.E. and Larson Å., Phys.Rev. A, **80**, 012501 (2009).
[3] Rubel M. J. et al. J. Phys: Conf. Ser. **100** 062028 (2008)
[4] Samm U. Trans. Fus. Scien.& Techn. Vol**. 49** 234-239 (2006).
[5] Shimomura Y. J. Nucl. Mater. **363-365** (2007) 467-475.
[6] Krasheninnikov S. Plasma Phys. Control. Fusion **53** 074017 (2011)
[7] Roth J. et al.Nucl.Instr. and Meth. in Phys.Res. B **258** 253-263 (2007).
[8] Giusti A., J.Phys.B, **13**, 3867-3894, (1980).
[9] Schneider I. F. , Rabadán I., Carata L. , Andersen L. H., Suzor-Weiner A. and Tennyson J., J. Phys. B: At. Mol. Opt. Phys. **33** 4849–4861 2000).
[10] Stroe et al. Rom.Rep. in Phys. Vol **57. 4**. 748-772 (2005).
[11] Motapon O. et al. Plasma Sources Sci. Technol **15** 23-32 (2006).
[12] Seaton M.J. Rep. Prog. Phys., Vol. **46** 167-257 (1983).
[13] Schneider I.F., Dulieu O., Giutsi-Suzor A.. & Roueff E., ApJ, **424** 983-987 1994).